Neuroradiology
https://doi.org/10.1007/s00234-020-02522-9

DIAGNOSTIC NEURORADIOLOGY

Validation of combined use of DWI and percentage signal recovery-optimized protocol of DSC-MRI in differentiation of high-grade glioma, metastasis, and lymphoma

Emetullah Cindil[1] · Halit Nahit Sendur[1] · Mahi Nur Cerit[1] · Nurullah Dag[1] · Nesrin Erdogan[1] · Filiz Elbuken Celebi[2] · Yusuf Oner[1] · Turgut Tali[1]

Received: 2 June 2020 / Accepted: 13 August 2020

Abstract

Purpose With conventional MRI, it is often difficult to effectively differentiate between contrast-enhancing brain tumors, including primary central nervous system lymphoma (PCNSL), high-grade glioma (HGG), and metastasis. This study aimed to assess the discrimination ability of the parameters obtained from DWI and the percentage signal recovery- (PSR-) optimized protocol of DSC-MRI between these three tumor types at an initial step.

Methods DSC-MRI using a PSR-optimized protocol (TR/TE = 1500/30 ms, flip angle = 90°, no preload) and DWI of 99 solitary enhancing tumors (60 HGGs, 24 metastases, 15 PCNSLs) were retrospectively assessed before treatment. rCBV, PSR, ADC in the tumor core and rCBV, and ADC in peritumoral edema were measured. The differences were evaluated using one-way ANOVA, and the diagnostic performance was evaluated using ROC curve analysis.

Results PSR in the tumor core showed the best discriminating performance in differentiating these three tumor types with AUC values of 0.979 for PCNSL vs. others and 0.947 for HGG vs. metastasis. The ADC was only helpful in the tumor core and distinguishing PCNSLs from others (AUC = 0.897).

Conclusion Different from CBV-optimized protocols (preload, intermediate FA), PSR derived from the PSR-optimized protocol seems to be the most important parameter in the differentiation of HGGs, metastases, and PCNSLs at initial diagnosis. This property makes PSR remarkable and carries the need for comprehensive DSC-MRI protocols, which provides PSR sensitivity and CBV accuracy together, such as the preload use of the PSR-optimized protocol before the CBV-optimized protocol.

Keywords DSC-MRI · Glioblastoma · Metastasis · Primary cranial nervous system lymphoma · DWI

Introduction

The characterization of brain tumors using conventional magnetic resonance imaging (MRI) in the pretreatment period is still inconclusive due to similar imaging patterns, particularly in solitary enhancing lesions. It is more critical to differentiate between high-grade glioma (HGG), metastasis, and primary central nervous system lymphoma (PCNSL), which show

✉ Emetullah Cindil
emetiyildirim@yahoo.com

Halit Nahit Sendur
hsendur@gmail.com

Mahi Nur Cerit
mahinurp@yahoo.com

Nurullah Dag
drndag.radiology@gmail.com

Nesrin Erdogan
dr.nesrin.erdogan@gmail.com

Filiz Elbuken Celebi
elbuken.filiz@gmail.com

Yusuf Oner
yusufoner18@yahoo.com

Turgut Tali
turgut.tali@gmail.com

[1] School of Medicine, Department of Radiology, Gazi University, Ankara, Turkey

[2] School of Medicine, Department of Radiology, Yeditepe University, Istanbul, Turkey

Published online: 21 August 2020

similar appearance on a conventional MRI as solitary enhancing lesions with peritumoral edema. Accurate diagnosis at the initial step is mandatory due to their different management settings [1, 2].

Diffusion-weighted imaging (DWI) gives information on cellular architecture, and several studies have also been applied to differentiate primary brain tumors [3–7]. DWI provides quantification of the physiologic alteration of water diffusion in tissue. This diffusion feature can be measured using an apparent diffusion coefficient (ADC). Malignant primary brain tumors may show restricted diffusion characterized by low ADC values due to the high cellularity rate and narrowing of the intercellular space [3–5]. Today, it is well known that PCNSLs tend to demonstrate lower ADC values compared with HGGs and metastases due to their histologic characteristics but with significant overlaps [4, 6, 8]. On the other hand, ADC measurements of the peritumoral edema of these three types of tumors revealed conflicting results [3, 6, 9]. Therefore, discrimination of these tumors may be difficult using ADC only.

Perfusion-weighted imaging (PWI) methods that allow for the characterization of microenvironmental changes at a capillary level have been used in the characterization of brain tumors [8]. Dynamic susceptibility contrast (DSC) MRI is the most widely used perfusion technique based on measuring T2* signal changes during the initial pass of contrast material [8, 10]. Relative cerebral blood volume (rCBV) obtained by dividing the cerebral blood volume (CBV) of the lesion to the CBV of normal-appearing white matter (NAWM) is the most commonly used metric in the differentiation of brain tumors [6–8, 11, 12]. rCBV correlates with tumor vascularity and relatedly with neoangiogenesis [13, 14], and it has been shown to increase with the glioma degree [14, 15]. The percentage of signal recovery (PSR) obtained from the time-signal curve is used to a lesser extent in tumor differentiation, but recent studies have shown that its diagnostic efficacy is not only higher than rCBV in glioma grading [16] but also in the differentiation of common intracranial malign lesions (HGG, metastasis, and PCNSL) [11, 12, 17, 18]. PSR reflects the combined interaction of blood-brain barrier (BBB) integrity and vascular permeability related to the tissue's histologic characteristics [19]. However, contrast leakage effects cause a decrease in the T2* signal reduction due to their T1-shortening effect, which then results in an underestimation of CBV [20, 21]. This concern has led to the development of new applications enabling accurate CBV, such as leakage-correction protocols using contrast preload [21], adapting image acquisition parameters to balance T1 and T2 sensitivity [22, 23], and postprocessing leakage-correction methods [15, 20]. However, the addition of a preload dose is thought to affect the PSR measurements, which have prominent diagnostic ability at initial diagnosis of intracranial tumors, especially in the discrimination of metastasis and HGG, which is the most challenging area [24]. Bell et al. [25] showed that PSR in HGGs decreases with increasing preload dose, which may reduce the variation between tumor groups. Boxerman et al. [26] also showed that the T1-sensitive protocol (high flip angle [FA] and short TE) caused increased PSR in HGGs, whereas the administration of preload contrast reduced the variation in PSR measured by different protocols. Likewise, Lee et al. [24] also suggested that adapting pulse sequence parameters by decreasing T1 sensitivity and preload contrast administration may suppress the PSR differences between these three types of tumors. Although PSR is very useful in distinguishing common intracranial tumors at initial diagnosis [11, 17, 18], CBV is indispensable, especially in distinguishing treatment response from residual or recurrent tumors and guiding surgical interventions [27, 28]. Therefore, there is a balance between PSR sensitivity and rCBV accuracy for DSR-MRI acquisition parameters. Recent studies on the differentiation of intracranial tumors have mostly used DSC-MRI protocols adapted for rCBV accuracy (i.e., preload contrast, intermediate FA, low TE, and postprocessing correction algorithm) [24] but not for PSR optimization. Although there are guidelines for implementation [8], the heterogeneity of inter-institutional protocols makes standardization difficult and prevents the cut-off value of perfusion parameters to be used for lesion discrimination.

As far as we know, there are only a few studies based on the differentiation between all three tumor types together (HGGs, PCNSLs, and metastases) using DSC-MRI [6, 17, 18, 24] but with different imaging algorithms. We aimed to determine whether using high FA values and low TE values for PSR optimization may provide better diagnostic performance in the differentiation of HGGs, PCNSLs, and metastases on the basis of the evaluation of both the enhancing tumor core and the surrounding T2-hyperintense edema at the initial diagnostic step, without using time-consuming protocols for CBV accuracy. Our second aim was to evaluate the contribution of DWI to the differentiation of these three types of tumors in the same aforementioned areas.

Materials and methods

Patient population

This retrospective study was made up of 99 consecutive patients with solitary enhancing brain tumors who underwent multiparametric MRI, including DWI and DSC-PWI prior to biopsy or surgery between March 2015 and June 2019. None of the patients have prior treatment history for brain tumors. We derived data from the institutional archive and included 60 HGGs (50 years ± 16), 24 metastases (57 years ± 12), and 15 PCNSLs (61 years ± 15), all being biopsy or surgery proven. Twelve metastases originated from lung cancer, 7 from breast

cancer, 2 from rectal cancer, 1 from thyroid cancer, 1 from gastric adenocarcinoma, and 1 from malign melanoma. All of the PCNSLs in the study were of diffuse large B cell type. HGGs consisted of 40 glioblastomas (GBs) (16 IDH-wild, 6 IDH-mutant, 18 NOS) and 20 anaplastic astrocytomas (8 IDH-wild, 8 IDH-mutant, and 4 NOS). All tumors were solitary enhancing lesions with surrounding edema. A local ethics committee approved this single-center retrospective study, and the requirement for informed consent was waived.

DWI and DSC-MRI acquisition

All examinations were performed at a 3T MR system (Magnetom Verio, Siemens Healthinieers, Erlangen, Germany) using an 8-channel head matrix coil. DSC-MRI was performed using a fast echoplanar T2-weighted gradient-echo sequence. The perfusion imaging parameters were as follows: 5 mm slice thickness with 1.5 mm intersection gap, 1500 ms for TR, 30 ms for TE, 90° FA, 23 cm FOV, 1.0 NEX, 128 × 128 matrix size, and 60 phases (25 axial slices). Image acquisition was obtained during a 10-s delayed bolus injection of Gadobutrol formula (0.1 mL/kg) (Gadovist, Bayer Health Care, Germany), followed by a 20 mL saline via a 20-gauge catheter placed in the antecubital vein with an automatic injector at a rate of 5 mL/sn. The total examination time was ~ 1 min 23 s, with a 1.38-s temporal resolution.

DWI was performed before DSC-MRI in the axial plane using a single-shot echoplanar imaging sequence with the following parameters: 3-mm slice thickness with no gap, 15,000 ms for TR, 90 ms for TE, 23 cm FOV, 2.0 NEX, 128 × 128 matrix size, diffusion gradient encoding in three orthogonal directions, $b = 1000$ s/mm^2, and scanning time 90 s.

Image processing and analysis

Data were transferred to a dedicated workstation and analyzed two neuroradiologists with more than 15 years of experience, blinded to the histologic data using in-house software. CBV values were obtained by placing ROIs (60–80 mm^2) on multiple hot spots (3–7) of the tumor core. T2-weighted, postcontrast T1-weighted images, and SWI images overlaid on CBV maps were used to ensure the correct position of the tumor core and also to exclude any hemorrhage, necrosis, calcification, or large vessels within ROIs. The highest values of CBV were selected, and the mean value of three measurements was recorded for analysis. Then, the measurement of CBV of the peritumoral area was applied in the same fashion. For normalization, ROIs with a similar size were placed in the contralateral NAWM, excluding gray matter. Finally, the rCBV was calculated by dividing the CBV of lesion or perilesional area to the CBV of NAWM.

To obtain PSR measurements, ROIs (60–80 mm^2) were drawn on the grayscale perfusion maps overlaid on postcontrast T1-weighted images. PSR values were calculated from the acquired perfusion curve of the tumor core and contralateral NAWM based on the following formula: PSR = (Spost-Smin) / (Spre-Smin) × 100% where Spre represents baseline signal intensity at the initial non-contrast fase, Smin the maximal drop value of signal intensity, and Spost the peak value after the signal recovery. The PSR of the tumor core was normalized to the values from the NAWM of the contralateral hemisphere in order to obtain relative PSR (rPSR). For all measurements, hemorrhagic, necrotic, and calcified regions were tried to exclude depending on T2-weighted, T1-weighted, and SWI images.

Measurements of ADC from the tumor core and peritumoral edema were performed on ADC maps. The mean ADC was obtained from the darkest areas with the ROI size in the range of 40–80 mm^2. Similar to perfusion evaluation, fused images were used to outline hemorrhage, necrosis, or calcification. After measuring the ROIs three times, the average value of the three measurements was taken.

Statistical analysis

All statistical analysis was performed using SPSS, version 23 (IBM, Chicago), and a p value less than 0.05 was accepted as the criterion of significance. All values are specified as mean ± standard deviation (SD). The differences in perfusion and diffusion parameters among HGGs, PCNSLs, and metastases were assessed using one-way analysis of variance (ANOVA), followed by the post hoc Tamhane test used for dual group comparisons. Student's t test was used for pairwise comparisons. The area under the curve (AUC) from receiver operating characteristic (ROC) analysis was used for each parameter to evaluate the diagnostic performance of parameters between groups. Optimal cut-off value was determined by Youden index. For evaluating the diagnostic performance of combination of parameters, logistic regression analysis was performed, if available.

Results

The mean values of perfusion metrics and the results of one-way of ANOVA are summarized in Table 1. The discriminating performances of PCNSL vs. HGG and metastasis and HGG vs. metastasis are summarized in Table 2. PSR came forward as the best discriminating parameter between these three types of tumors, including high levels in PCNSLs, intermediate levels in HGGs, and low levels in metastases (Table 2; Figs. 1, 2, and 3).

Table 1 Mean values, standard deviations, and ranges (in parentheses) of perfusion and diffusion parameters and comparisons of groups using ANOVA test

Parameter	HGG	Metastasis	PCNSL	*P* values (ANOVA)
rCBV	4.01 ± 2.51 (1.56–13.89)	4.25 ± 3.05 (1.87–15.71)	1.51 ± 0.45 (0.65–2.37)	0.001*
rCBV-edema	1.61 ± 0.99 (0.49–6.60)	0.77 ± 0.31 (0.22–1.52)	0.89 ± 0.32 (0.36–1.64)	< 0.001*
PSR	95.30 ± 20.12 (65.91–197.22)	59.83 ± 15.21 (34.41–94.17)	164.05 ± 37.0 (113.16–243.78)	< 0.001*
rPSR	1.16 ± 0.59 (0.59–3.5)	0.71 ± 0.20 (0.43–1.34)	1.81 ± 0.39 (1.36–2.56)	< 0.001*
ADC ($\times 10^{-3}$ mm^2/s)	0.930 ± 0.212 (0.502–1.464)	0.981 ± 0.231 (0.550–1.414)	0.656 ± 0.127 (0.481–0.894)	< 0.001*
ADC-edema ($\times 10^{-3}$ mm^2/s)	1.230 ± 0.256 (0.594–1.835)	1.518 ± 0.513 (0.713–2.565)	1.617 ± 0.321 (1.191–2.324)	< 0.001*
Pairwise comparison with post hoc Tamhane test–*P* values				
Parameter	**HGG vs MET**	**HGG vs PCNSL**	**PCNSL vs MET**	
rCBV	0.919	< 0.001*	0.001*	
rCBV-edema	< 0.001*	0.010*	0.894	
PSR	< 0.001*	< 0.001*	< 0.001*	
rPSR	< 0.001*	0.001*	< 0.001*	
ADC	0.731	< 0.001*	< 0.001*	
ADC-edema	0.041*	0.001*	0.847	

ADC apparent diffusion coefficient, *HGG* high-grade glioma, *MET* metastasis, *PCNSL* primary cranial nervous system lymphoma, *rCBV* relative cerebral blood volume, *PSR* percentage signal recovery, *rPSR* relative percentage signal recovery

* Significant

PCNSL vs. metastasis and HGG

Compared with metastases and HGGs, PCNSLs showed significantly lower values of rCBV and ADC, as well as significantly higher PSR and rPSR values in the tumor core (Table 1; Figs. 1, 2, and 3). PSR in the tumor core had the best discriminating performance with an AUC of 0.979, and the rCBV was the second one with an AUC of 0.970 in the differentiation of PCNSLs from others (Table 2, Fig. 4). The accuracy rates were 0.95 at the cut-off value of 112 for PSR and 0.94 at the cut-off value of 1.94 for rCBV (Table 2). The combination of PSR and rCBV did not improve diagnostic accuracy (0.94), sensitivity (0.97), or specificity (0.93) value. ADC in the tumor core showed slight overlaps between PCNSLs vs. HGGs and metastases; thus, the AUC value (0.879) was lower compared with PSR and rCBV. In the tumor core, the combination of PSR and ADC, as well as rCBV and ADC slightly increased the diagnostic performances, with AUC values of 0.986 (95% CI, 0.968–1.00) and 0.990 (95% CI, 0.973–1.00), respectively ($p < 0.001$), compared with the individual evaluation of each parameter alone. On the other hand, none of the ADC and rCBV values obtained from the

Table 2 Diagnostic performance of each perfusion parameter in differentiation of PCNSL versus MET and HGG, and HGG versus MET

Parameter	HGG vs MET						PCNSL vs others					
	AUC (95% CI)	*P* value	Cut-off	SEN	SPE	Accuracy	AUC (95% CI)	*P* value	Cut-off	SEN	SPE	Accuracy
rCBV	0.501 (0.359–0.643)	0.988	-	-	-	-	0.970 (0.936–1.0)	< 0.001*	1.94	0.94	0.93	0.94
rCBV-edema	0.873 (0.795–0.950)	< 0.001*	1.13	0.75	0.87	0.77	0.691 (0.573–0.809)	0.019*	0.99	0.64	0.67	0.64
PSR	0.947 (0.893–1.0)	< 0.001*	74.25	0.92	0.85	0.92	0.979 (0.953–1.0)	< 0.001*	112	1.00	0.93	0.95
rPSR	0.861 (0.794–0.962)	< 0.001*	0.82	0.85	0.83	0.86	0.907 (0.842–0.961)	< 0.001*	1.35	1.00	0.87	0.89
ADC	0.566 (0.426–0.705)	0.349	-	-	-	-	0.879 (0.797–0.961)	< 0.001*	0.758	0.76	0.80	0.77
ADC-edema	0.670 (0.525–0.814)	0.015*	1258	0.75	0.57	0.62	0.763 (0.644–0.883)	0.001*	1.381	0.73	0.69	0.72

ADC apparent diffusion coefficient, *HGG* high-grade glioma, *MET* metastasis, *PCNSL* primary cranial nervous system lymphoma, *AUC* area under the curve, *CI* confidence interval, *SEN* sensitivity, *SPE* specificity, *rCBV* relative cerebral blood volume, *PSR* percentage signal recovery, *rPSR* relative percentage signal recovery

* Significant

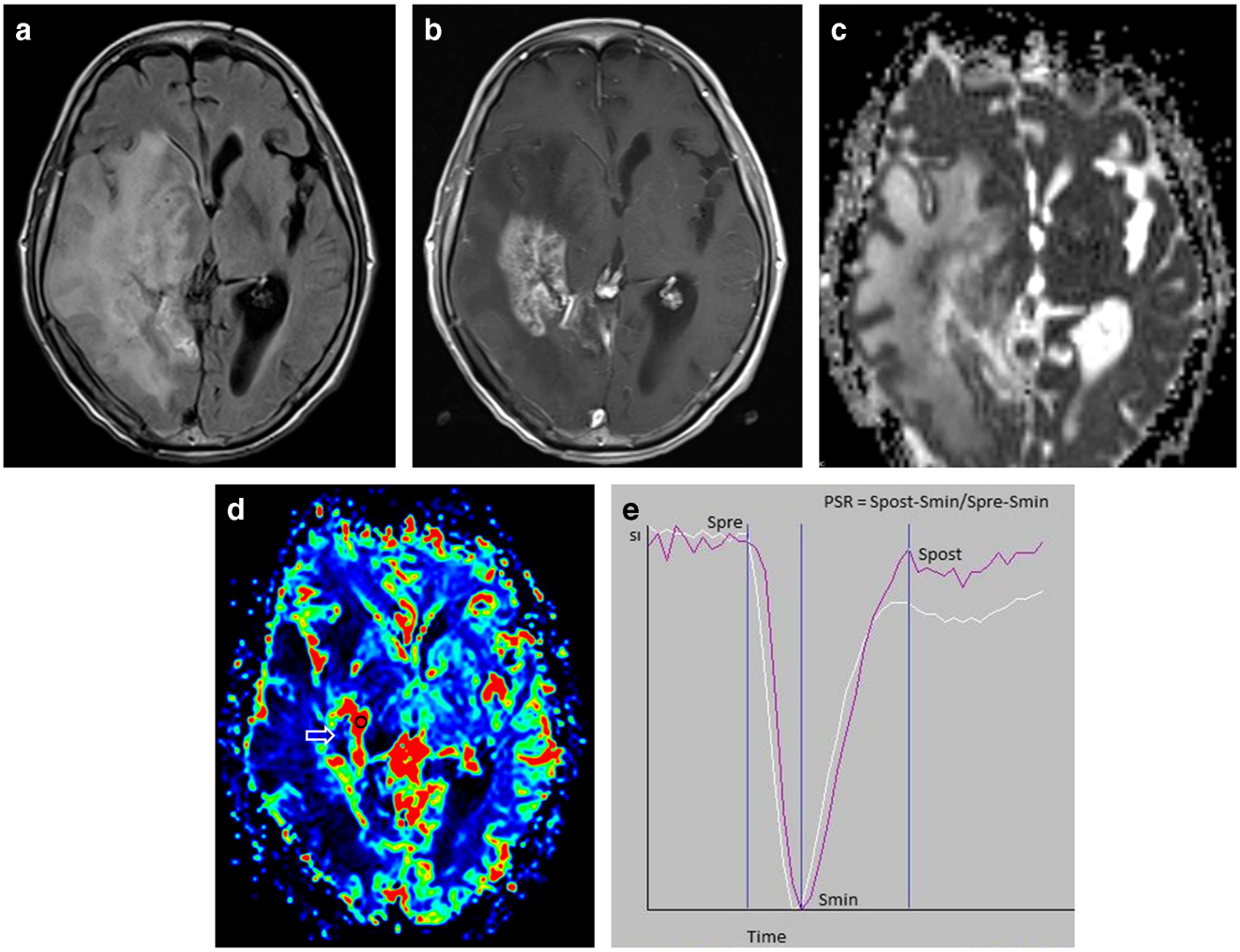

Fig. 1 A 58-year-old woman with histologically proved glioblastoma (isocitrate dehydrogenase wild type). The T2-weighted FLAIR image (**a**) shows oval-shaped mass in the right temporo-occipital region and thalamus with extensive perilesional edema. The contrast-enhanced T1-weighted image (**b**) demonstrates heterogeneous dense contrast enhancement. The ADC map (**c**) shows peripherally scattered hypointense areas representing high cellularity (0.988×10^{-3} mm^2/s). The cerebral blood volume map (**d**) demonstrates increased perfusion in tumor core with rCBV at 6.25 (small black ROI on hot spot). Signal intensity-time curve (**e**) shows that the curve returns close to baseline after the first pass with the percentage signal recovery being 95.92 (pink line represents tumor core, white line represents the automatic correction of software)

peritumoral zone had an efficient discriminating characteristic between similar groups (Table 3). Furthermore, in pairwise analysis, the mean rCBV of HGGs in the peritumoral zone was significantly higher than the mean value of PCNSLs (p = 0.010), whereas the values of metastasis and PCNSLs did not show any significant differences ($p > 0.05$) (Table 1).

HGG vs metastasis

ADC and rCBV in the tumor core did not show any statistically significant differences between HGGs and metastases ($p > 0.05$) (Tables 1 and 2). Both PSR and rPSR were significantly higher in HGGs than those in metastases (95.30 vs 59.83 for PSR; 1.16 vs 0.71 for rPSR, respectively) (Table 1). Compared with rPSR, PSR showed a higher AUC value of 0.947 with an accuracy of 0.92 at the cut-off point of 74.25 (Table 2). In the peritumoral region, compared with metastases, HGGs showed significantly higher values of rCBV with slight overlaps (mean values 0.77 ± 0.31 for metastases, 1.61 ± 0.99 for HGGs; AUC of 0.873, and accuracy of 0.77 at the optimal cut-off value of 1.13) (Tables 1 and 2, Fig. 5). Moreover, the combination of PSR from the tumor core and rCBV from the peritumoral region slightly increased the diagnostic performance with an AUC of 0.971 (95% CI, 0.929–1.00), accuracy of 0.94, sensitivity of 0.95, and specificity of 0.91 compared with the evaluation of each parameter alone (Fig. 5). Although peritumoral ADC values in HGGs (1.230×10^{-3} mm^2/s) were revelaed to be relatively lower than the values in metastases (1.518×10^{-3} mm^2/s), there were significant overlaps between these two groups (AUC =

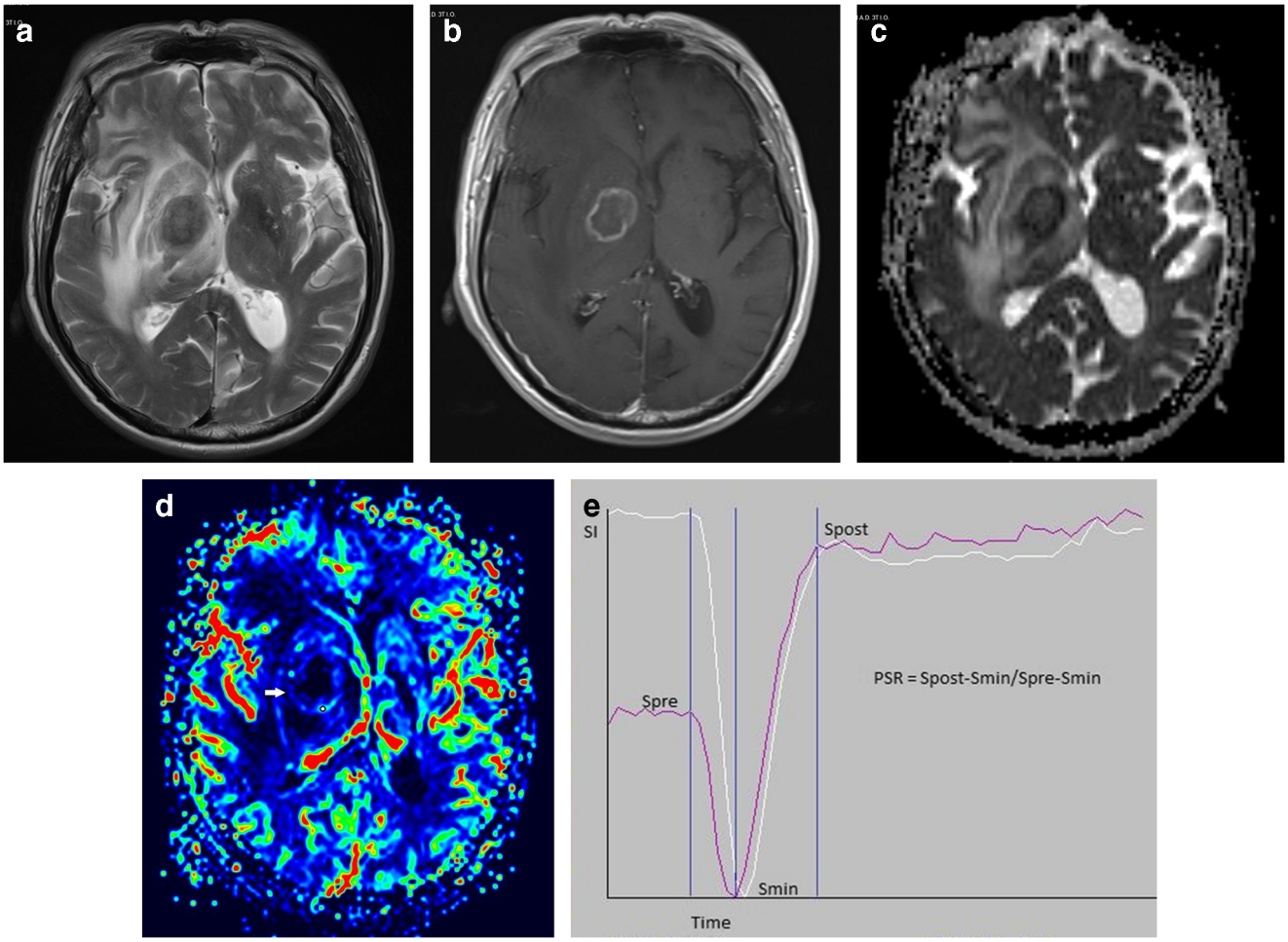

Fig. 2 A 52-year-old man with primary cranial nervous system lymphoma. The T2-weighted axial image (**a**) shows round shape hypointense mass in the right basal ganglia with extensive perilesional edema. The contrast-enhanced axial T1-weighted image (**b**) demonstrates ring-like enhancement. The ADC map (**c**) shows prominent diffusion restriction in the tumor core (0.603×10^{-3} mm^2/s). The cerebral blood volume map (**d**) demonstrates slightly increased perfusion on tumor area and the measured rCBV value is 1.32 (small black ROI on hot spot). Signal intensity-time curve (**e**) shows that the curve of tumor area markedly exceeds the baseline after the first pass with the percentage signal recovery being 223.58 (pink line represents tumor core, white line represents automatic correction of software)

0.670). The combination of PSR from the tumor core and ADC from peritumoral edema did not have an impact on the diagnostic performance (AUC = 0.945, 95% CI 0.881–1.00).

Discussion

PCNSL, HGG, and metastases may present similar on conventional MRI, but accurate diagnosis at the initial step is important in regard to treatment planning. Although PCNSL shows some characteristic findings on conventional MRI, it may not always be possible to distinguish it from HGG and metastasis when atypical features, such as necrosis, bleeding, or heterogeneous enhancement, are present. In this study, we firstly focused on the utility of diffusion and perfusion metrics of the tumor core and found statistically significant lower rCBV and ADC, as well as higher PSR and rPSR values in PCNSLs, compared with values measured from HGGs and metastasis. Those were in agreement with the previous studies [4, 6, 7, 12, 17, 18, 24, 29, 31, 32], with PSR being the most predictive among other metrics (AUC of 0.979, sensitivity of 1.0, specificity of 0.93, and accuracy of 0.95). In pairwise analyses, PSR and rPSR values in the tumor core were also effective in discriminating HGGs from metastases (AUC of 0.947 and 0.861, respectively), whereas rCBV and ADC did not show any significant difference.

Lymphomas are characterized as dense cellularity and tend to grow around the perivascular region and at the outer border of the vessel wall, which has been shown to be infiltrated and destroyed by tumor cells without prominent neovascularization [8, 33, 34]. Thus, lymphomas show a higher degree of BBB disruption than HGGs, whereas the basement membrane integrity of HGGs is preserved [33]. Based on these findings, although PCNSLs show higher permeability and much more contrast extravasation to the interstitial space, T1 and T2* shortening effects are not evident at the time of the first pass

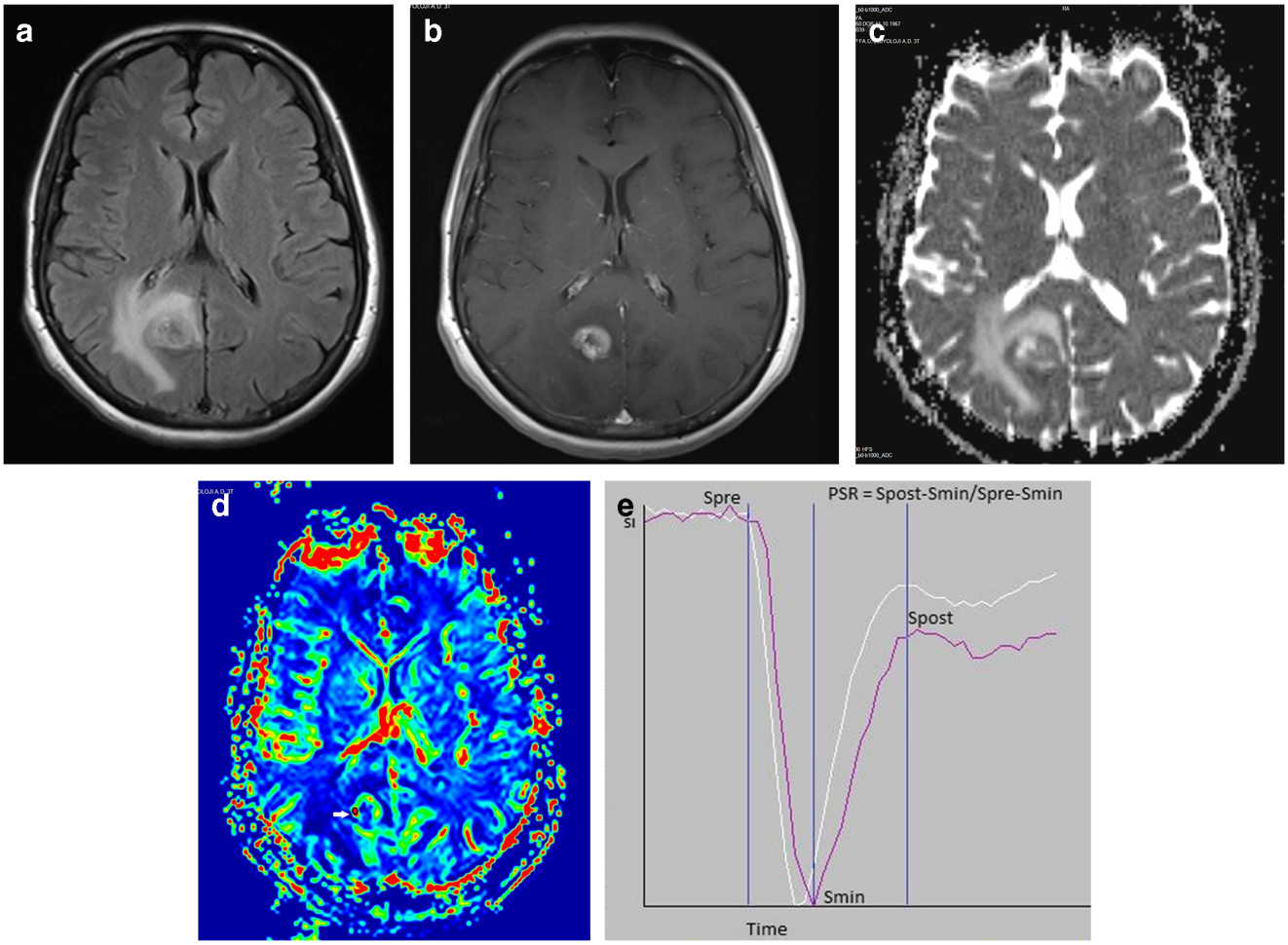

Fig. 3 A 65-year-old woman with a right occipital metastasis from breast cancer. The T2-weighted FLAIR image (**a**) shows round shape lesion with perilesional edema. The post-contrast axial T1-weighted image (**b**) demonstrates heterogeneous enhancement. The ADC map (**c**) shows hypointense areas in the tumor area (0.883×10^{-3} mm^2/s). The cerebral blood volume map (**d**) shows ring-like slightly increased perfusion with rCBV at 2.12 (small black ROI on hot spot). Signal intensity-time curve (**e**) shows that the curve ends far to baseline after the first pass with the percentage signal recovery being 61.25 (pink line represents tumor core, white line represents automatic correction of software)

due to the slow and late accumulation of contrast in PCNSLs, but the T1 shortening effect dominates the T2* shortening effect immediately after the first pass and causes higher signal recovery values in the signal time curve exceeding the basal level when compared with HGGs [32]. Hartman et al. [34] also suggested that due to the hybrid effect of low CBV, the signal decline in PCNSL was less in the first pass, and then, they observed a higher signal recovery due to the higher contrast leakage than GBs. In HGG and metastasis, which show high microvascular density, the T2* effect resulting from the accumulation of a fast and abundant contrast agent in the extracellular extravascular space is significantly higher than the T1 shortening effect during and after the first transition period, resulting in a lower PSR [18]. Furthermore, metastases exhibit prominent capillary fenestration, open endothelial junctions, and a complete lack of BBB, and relatedly, they are expected to show more and faster contrast extravasation to the extravascular extracellular space than HGGs. Therefore, signal recovery is expected to be less in metastases. The differences in PSR between these three tumor types may be explained by complex integration of differences in capillary architecture, permeability, cellular features, and microvessel density [19, 34]. On the other hand, studies using leakage-correction protocols with preload to obtain accurate CBV value have reported a lower diagnostic ability of PSR [24] between these three tumor types. The main purpose of the preloading dosage is to reduce local tissue T1 to an appropriate extent so that subsequent contrast injections only cause minor additional T1 changes and thereby increase sensitivity to expected T2* changes. As is known, PSR depends dominantly on contrast leakage effects that cause T1 shortening. Decreased T1 changes at the cellular level with preload or adapting pulse sequence parameters (low TE and intermediate FA) may diminish the PSR values and diminish the variations in PSR values between tumor groups [24–26].

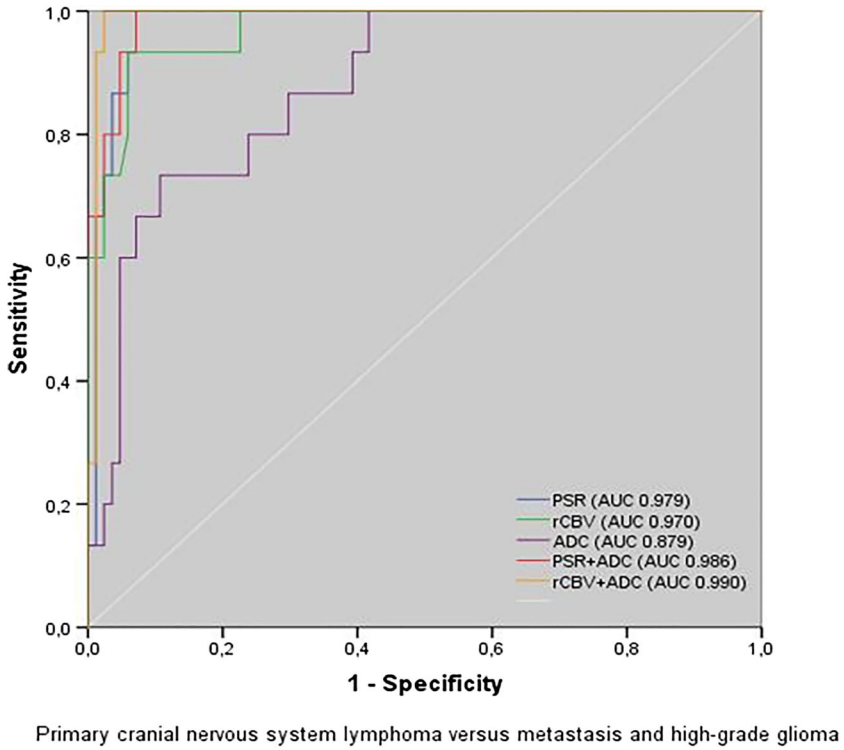

Fig. 4 Receiver operating characteristic curves of percentage signal recovery (PSR), relative cerebral blood volume (rCBV), apparent diffusion coefficient (ADC), the combinations of PSR and ADC, and rCBV and ADC from tumor core in differentiating primary cranial nervous system lymphoma from high-grade gliomas and metastases

PCNSLs also tend to show little neoangiogenesis, whereas HGGs and metastases show increased angiogenesis and perfusion [17, 28, 29, 32]. Accordingly, rCBV in PCNLSs (1.51 ± 0.45) was significantly lower than those in HGGs (4.01 ± 2.51) and metastases (4.25 ± 3.05) and had nearly the same powerful distinguishing ability with PSR in this study (AUC of 0.970). However, a few studies using a preload bolus contrast technique or correction of rCBV during postprocessing reported relatively higher rCBV values for lymphomas [7, 12, 17, 31]. Using these techniques, PCNSLs show hyperperfusion characteristics that hinder differentiation of them from other hypervascular tumors such as HGGs and metastases. Of interest, Nakajima et al. [12] and Toh et al. [31] showed lower diagnostic performance for corrected rCBV compared with uncorrected rCBV in distinguishing PCNSLs from GBs.

In pairwise analysis, rCBV in the tumor core did not show any significant differences between HGG and metastasis. Both had high rCBV values nearly at the same level, reflecting increased perfusion consistent with the studies using preload or no-preload techniques that hinder the discrimination among tumor types [6, 9, 24, 30]. Contradictory to this assumption, Mangla et al. [17] showed significantly higher rCBV values in HGGs than in metastases. Patient groups' heterogeneity and differences in the acquisition and analysis protocol may be the causes of this conflict. In this context, PSR in the tumor core has come to the front as the best distinguishing parameter, with an AUC of 0.947, in the differentiation of HGG from metastasis, which may help to discriminate each group with an accuracy rate of 0.92, as seen in the differentiation of PCNSLs from others in this present study. These findings were consistent with previous results [11, 17, 18], which used a similar no-preload technique but with different TE and FA values (Table 3). For example, Vallee et al. [18], who used a similar DSC protocol, except for a higher TR value (1980 ms), demonstrated statistically significant differences for PSR in the differentiation of metastasis from PCNSLs and GBs with an AUC of 0.969. In addition, the mean PSR values of HGGs and lymphomas (95.3 and 164.05, respectively) are quite similar to the results of Liao et al. [29] (93 and 175, respectively), who used identical imaging parameters (no preload, 1440 TR, 30 TE, 90 FA) to our study. Mangla et al. [17] used a PSR-optimized acquisition protocol (Table 3) (no preload, high FA = 80, intermediate TE = 50 ms) and reported PSR to have a higher AUC value (0.880 for mean PSR) than rCBV (AUC of 0.759) in the differentiation of PCNSLs from metastases and GBs, despite the usage of a postprocessing CBV correction algorithm. In the differentiation of GB from metastasis, the reported diagnostic ability of PSR was very close (AUC value of 0.938 for mean PSR) to this study [17]. Conversely, a newer study [24] that used a DSC protocol designed for rCBV accuracy (with preload, intermediate FA = 60° and low TE = 40 ms) and a postprocessing leakage-correction algorithm (Table 3) reported markedly lower diagnostic performance for both rCBV and PSR (AUC of 0.66–0.83) in the discrimination of PCNSLs from others compared with our study. For GB vs. metastasis, they reported no significant differences for

Table 3 DSC-MR imaging parameters of some studies in literature

Study (year)	HGG (*n*)	MET (*n*)	PCNSL (*n*)	Magnet strength (T)	Temporal resolution (ms)	Slice thickness (mm)	Preload gadolinium-based contrast agent	TR (ms)	TE (ms)	FA (degree)	Postprocessing leakage correction for CBV
Neska-Matuszewska (2018) [6]	27	30	17	1.5	1.26	8	No	1900	80	NA	No
Lee et al. (2019) [24]	14	20	7	1.5	1.16	5	Yes	1290	40	60	Yes
Cha et al. (2007) [11]	27GB	16		1.5	1.25	3-5	No	1000-1250	54	35	No
Mangla et al. (2011) [17]	22	22	22	1.5	NA	6	No	1500	50	80	Yes
Liao et al. (2008) [29]	11		9	1.5	1.5	5	No	1440	30	90	No
Nakajima et al. (2015) [12]	18		10	3	2	3	No	2000	30	90	Yes
Askaner et al. (2018) [30]	38 GB	76		3	NA	5	No	1400	32	NA	Yes
Makino et al. (2017) [7]	54 GB		33	3	1.17	5	Yes	1400	32	60	No
Toh et al. (2013) [31]	20 GB		15	3	1.28	4	No	1640	40	90	Yes
Vallee et al. (2018) [18]	14 GB	13	28	3	NA	4	No	1980	30	90	No
Xing et al. (2014) [32]	26		12	3	1.6	NA	No	1500	30	NA	No

HGG high-grade glioma, *MET* metastasis, *PCNSL* primary cranial nervous system lymphoma, *GB* glioblastoma, *TR* time to repetition, *TE* time to echo, *FA* flip angle, *DSC* dynamic susceptibility contrast-enhanced, *NA* not available

both rCBV and PSR [24]. On the other hand, although it has been known that rCBV has the ability to differentiate lymphoma from others, the reported diagnostic distinguishing ability of rCBV in some of these publications was even lower than the one in our own study [12, 17, 24]. Only Neska-Matuszewska et al. [6], who used a protocol with a weight of T2 (TR 1900 ms, TE 80 ms, without identifying FA) for a similar patient group, reported accuracy values that were slightly higher for rCBV (0.98) and lower for rPSR (0.86) without identifying AUC values in the differentiation of PCNSLs from others, but they reported no statistically significant difference for rPSR between GBs and metastases. In our study, the use of a T1-weighted protocol probably increased the PSR variation in tumor groups for particular differentiation of HGGs from metastasis and provided better results. However, better results for rCBV in the differentiation of PCNSLs from others could not be explained depending on acquisition parameters, since only a small patient number of other studies may be the cause of this inconsistency.

Furthermore, we also evaluated the rCBV of lesion groups' peritumoral edema. HGG revealed a significant increase in rCBV compared with metastases verifying the peritumoral infiltrative pattern of HGG. Neoangiogenesis characterized by newly formed, structurally abnormal serpentine vessels induces leaky capillaries [35] and is the major cause of rCBV increase in the peritumoral area of HGGs [6, 9, 30, 36, 37]. Metastases do not show a common infiltrative growth pattern, and thus, peritumoral edema is thought to be completely vasogenic [38] and caused by tumor expansion due to displacement of the parenchyma. In distinguishing HGG from metastasis, the AUC value of rCBV in the peritumoral area was 0.873, which is consistent with previous results [6, 9, 17, 30, 36], but there was a moderate overlap between two groups. In accordance with these results, when we combined PSR from the tumor core and rCBV from peritumoral edema, the diagnostic ability (AUC of 0.971, sensitivity of 0.95, specificity of 0.91, and accuracy of 0.94) increased slightly, which suggested that the combination may provide a partial impact for the discrimination of metastases from HGGs.

The results of ADC values in the tumor core between groups seem to be useful only in the discrimination of PCNSLs from others, not for HGGs from metastases, in accordance with previous results [4, 6, 7]. Higher tumor cell density and cellularity with narrow interstitial space are known to be the major cause of lower ADC values in PCNSLs compared with those in other types of tumors. However, the AUC value of 0.879 in this study revealed slight overlaps between PCNSLs vs. others, which is consistent with previous results [4, 6]. Thus, the measurement of ADC in tumor core, which is easily accessible and does not require a time-consuming procedure, may be used as an adjunct tool with other perfusion metrics in the differentiation of PCNSLs from others. Due to the infiltrative growth pattern,

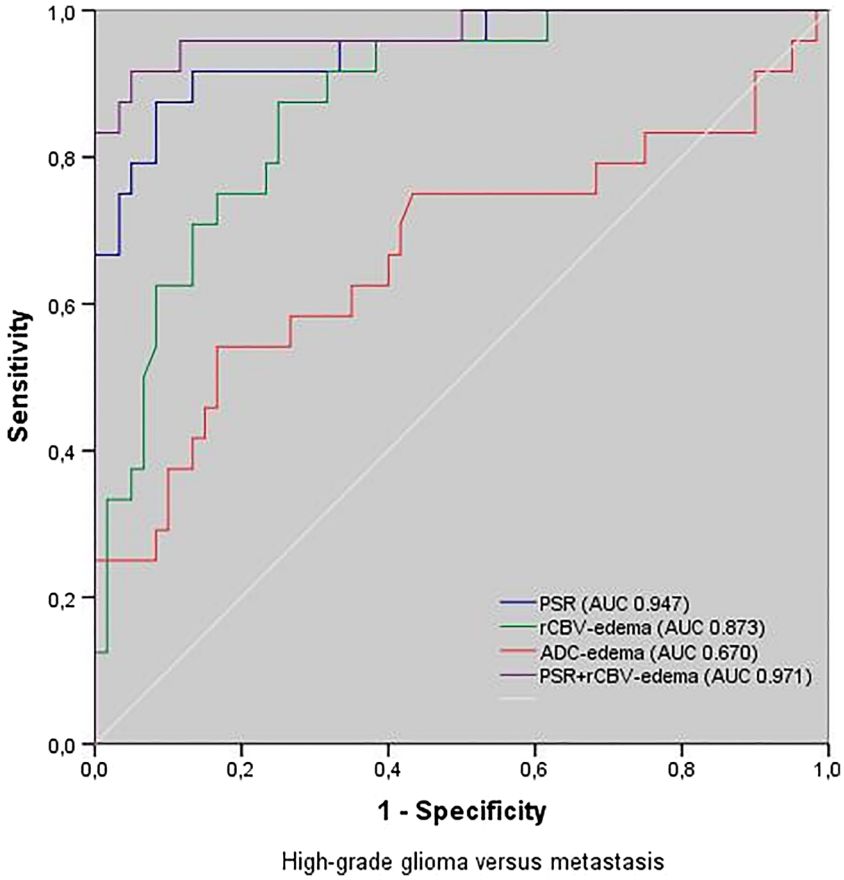

Fig. 5 Receiver operating characteristic curves of percentage signal recovery (PSR) from tumor core, relative cerebral blood volume (rCBV-edema) and apparent diffusion coefficient (ADC-edema) from perilesional edema, and combination of PSR and rCBV-edema in differentiating high-grade gliomas from metastases

the peritumoral edema is expected to show lower ADC values in HGGs compared with those in other tumors, but ADC of peritumoral edema did not show any impact on the discrimination of these three types of tumors in this study. Similarly, several studies in the literature [3, 6, 9] have reported that the contribution of ADC in the peritumoral region is still limited. Therefore, it is evident that the utility of ADC of the peritumoral region in the discrimination of HGGs from other tumors remains controversial and requires further validation with larger groups.

Although guidelines exist, there is no consensus on the optimal DSC-MR imaging methodology for the initial diagnostic phase of brain tumors. All approaches for the correction of the contrast leakage effect seem to diminish the PSR differences, especially between HGG and metastasis, which is the most challenging area in clinical practice [24]. Based on our findings, PSR calculation in the tumor core appears to be more effective than rCBV at the initial step of discriminating HGGs and metastases. PSR is also a parameter that is easier to measure than rCBV in perfusion imaging because it does not require sophisticated software or detailed postprocessing procedures [7]. Given that the boot affects of both PSR and CBV, DSC-MR imaging protocols that maintain rCBV accuracy and PSR sensitivity without preloading may be useful. Of interest, Semmineh et al. [39] recently reported a protocol providing very accurate predictions of rCBV without preload or lower preload dosage but that requires the use of a low FA (30°) to reduce T1 weight. However, they did not identify the effects of the protocol on PSR. Bell et al. [25] also showed that CBV measurements did not vary between preloading quantities, including no-preload option (TR of 2000 ms, TE of 20 ms, and FA of 60°) with the postprocessing correction of CBV in HGGs. Comprehensive DSC protocols are still needed to enable both PSR optimization and CBV accuracy. The use of PSR-optimized imaging (low TE, high FA, and no preload) as the preload of the CBV-optimized protocol (adapting pulse sequences: low TE, intermediate FA, and preload), including postprocessing correction algorithms, has been suggested by some authors [8, 26]. In addition, multi-echo DSC-MRI protocols have been recently launched, which combine simultaneous spin-gradient-echo acquisitions at different TE levels to eliminate T1 effects without preload for accurate rCBV estimation and to obtain balanced T1 and T2 weighting for PSR calculation that may help provide tumor differentiation [22, 40, 41].

There are some limitations to this study. The retrospective nature of the study may have caused selection bias. Although this study consists of a higher number of patients than the studies based on similar issues in the literature, the number of patients with lymphoma is relatively low compared with other groups. Comprehensive studies including other MRI characteristics in larger cohorts may provide a new

perspective to the diagnostic approach. We also did not differentiate metastases by primary tumor type due to unequal distribution. Further studies that encompass a wider cohort and equal distribution of tumor groups are warranted.

Conclusion

The analysis of perfusion parameters is essential in differentiating between HGGs, metastases, and PCNSLs. The diagnostic performance of PSR, an easily measured parameter, seems to be significantly effective at the time of initial diagnosis. Although preload contrast administration provides more accurate rCBV values, due to the suppressing effect on PSR differences in these three tumor types, it may be more useful to use the protocols that maintain PSR sensitivity and CBV accuracy in the differentiation of mostly seen primary brain tumors, especially HGG vs. metastasis. Multi-echo acquisitions or preload administration of the PSR-optimized protocol before the CBV-optimized protocol are the suggesting methods for this content. Without sacrificing PSR, the standardization of the DSC-MRI protocol, combining PSR optimization and CBV accuracy together, may provide a great impact on perfusion imaging and tumor characterization. The diffusion parameters of the tumor area may also provide additional information, specifically in the differentiation of PCNSLs from HGGs and metastases.

Funding information No funding was received for this study.

Compliance with ethical standards

Conflict of interest The authors declare that they have no confilict of interest.

Ethical approval All procedures performed in studies involving human participants were in accordance with the ethical standards of the institutional and/or national research commitee and with the 1964 Helsinki Declaration and its later amendments or compareble ethical standards.

Informed consent As this is a retrospective study, formal consent is not required.

Abbreviations ADC, apparent diffusion coefficient; ANOVA, analysis of variance; AUC, area under the curve; BBB, blood brain barrier; CI, confidence interval; DWI, diffusion-weighted imaging; DSC, dynamic susceptibility-weighted contrast-enhanced; FA, flip angle; GB, glioblastoma; NAWM, normal-appearing white matter; PCNSL, primary cranial nervous system lymphoma; PSR, percentage signal recovery; rCBV , relative cerebral blood volume; ROC, receiver operating characteristic; SI, signal intensity

References

1. Omuro A, DeAngelis LM (2013) Glioblastoma and other malignant gliomas: a clinical review. JAMA 310:1842–1850
2. Stupp R, Mason WP, van den Bent MJ, Weller M, Fisher B, Taphoorn MJ, Belanger K, Brandes AA, Marosi C, Bogdahn U, Curschmann J, Janzer RC, Ludwin SK, Gorlia T, Allgeier A, Lacombe D, Cairncross JG, Eisenhauer E, Mirimanoff RO, European Organisation for Research and Treatment of Cancer Brain Tumor and Radiotherapy Groups, National Cancer Institute of Canada Clinical Trials Group (2005) Radiotherapy plus concomitant and adjuvant temozolomide for glioblastoma. N Engl J Med 352:987–996
3. Lee EJ, terBrugge K, Mikulis D, Choi DS, Bae JM, Lee SK, Moon SY (2011) Diagnostic value of peritumoral minimum apparent diffusion coefficient for differentiation of glioblastoma multiforme from solitary metastatic lesions. Am J Roentgenol 196:71–76
4. Doskaliyev A, Yamasaki F, Ohtaki M, Kajiwara Y, Takeshima Y, Watanabe Y, Takayasu T, Amatya VJ, Akiyama Y, Sugiyama K, Kurisu K (2012) Lymphomas and glioblastomas: differences in the apparent diffusion coefficient evaluated with high b-value diffusion-weighted magnetic resonance imaging at 3T. Eur J Radiol 81:339–344
5. Kono K, Inoue Y, Nakayama K, Shakudo M, Morino M, Ohata K, Wakasa K, Yamada R (2001) The role of diffusion-weighted imaging in patients with brain tumors. Am J Neuroradiol 22:1081–1088
6. Neska-Matuszewska M, Bladowska J, Sąsiadek M, Zimny A (2018) Differentiation of glioblastoma multiforme, metastases and primary central nervous system lymphomas using multiparametric perfusion and diffusion MR imaging of a tumor core and a peritumoral zone-searching for a practical approach. PLoS One 13(1):e0191341
7. Makino K, Hirai T, Nakamura H, Kuroda JI, Shinojima N, Uetani H, Kitajima M, Yano S (2018) Differentiating between primary central nervous system lymphomas and glioblastomas: combined use of perfusion-weighted and diffusion-weighted magnetic resonance ımaging. World Neurosurg 112:e1–e6
8. Welker K, Boxerman J, Kalnin A, Kaufmann T, Shiroishi M, Wintermark M, for the American Society of Functional Neuroradiology MR Perfusion Standards and Practice Subcommittee of the ASFNR Clinical Practice Committee (2015) American Society of Functional Neuroradiology MR Perfusion Standards and Practice Subcommittee of the ASFNR Clinical Practice Committee. ASFNR recommendations for clinical performance of MR dynamic susceptibility contrast perfusion imaging of the brain. AJNR Am J Neuroradiol 36:E41–E51
9. Tsougos I, Svolos P, Kousi E et al (2012) Differentiation of glioblastoma multiforme from metastatic brain tumor using proton magnetic resonance spectroscopy, diffusion and perfusion metrics at 3 T. Cancer Imaging 26:423–436
10. Shiroishi MS, Castellazzi G, Boxerman JL, D'Amore F, Essig M, Nguyen TB, Provenzale JM, Enterline DS, Anzalone N, Dörfler A, Rovira À, Wintermark M, Law M (2015) Principles of T2*-weighted dynamic susceptibility contrast MRI technique in brain tumor imaging. J Magn Reson Imaging 41:296–313
11. Cha S, Lupo JM, Chen MH et al (2007) Differentiation of glioblastoma multiforme and single brain metastasis by peak height and percentage of signal intensity recovery derived from dynamic susceptibility-weighted contrast-enhanced perfusion MR imaging. AJNR Am J Neuroradiol 28:1078–1084
12. Nakajima S, Okada T, Yamamoto A, Kanagaki M, Fushimi Y, Okada T, Arakawa Y, Takagi Y, Miyamoto S, Togashi K (2015) Differentiation between primary central nervous system lymphoma and glioblastoma: a comparative study of parameters derived from dynamic susceptibility contrast-enhanced perfusion-weighted MRI. Clinical Radiology 70:1393–1399
13. Jain RK, Di Tomaso E, Duda DG et al (2007) Angiogenesis in brain tumours. Nat Rev Neurosci 8:610–622

14. Sugahara T, Korogi Y, Kochi M, Ikushima I, Hirai T, Okuda T, Shigematsu Y, Liang L, Ge Y, Ushio Y, Takahashi M (1998) Correlation of MR imaging-determined cerebral blood volume maps with histologic and angiographic determination of vascularity of gliomas. AJR Am J Roentgenol 171(6):1479–1486
15. Boxerman JL, Schmainda KM, Weisskoff RM (2006) Relative cerebral blood volume maps corrected for contrast agent extravasation significantly correlate with glioma tumor grade, whereas uncorrected maps do not. AJNR Am J Neuroradiol 27:859–867
16. Aprile I, Giovannelli G, Fiaschini P, Muti M, Kouleridou A, Caputo N (2015) High- and low-grade glioma differentiation: the role of percentage signal recovery evaluation in MR dynamic susceptibility contrast imaging. Radiol Med 120(10):967–974
17. Mangla R, Kolar B, Zhu T, Zhong J, Almast J, Ekholm S (2011) Percentage of signal recovery derived from MR dynamic susceptibility contrast imaging is useful to differentiate common enhancing malignant lesions of the brain. Am J Neuroradiol 32:1004–1010
18. Vallée A, Guillevin C, Wager M, Delwail V, Guillevin R, Vallée JN (2018) Added value of spectroscopy to perfusion mrı in the differential diagnostic performance of common malignant brain tumors. AJNR Am J Neuroradiol 39(8):1423–1431
19. Semmineh NB, Xu J, Skinner JT, Xie J, Li H, Ayers G, Quarles CC (2015) Assessing tumor cytoarchitecture using multiecho DSC-MRI derived measures of the transverse relaxivity at tracer equilibrium (TRATE). Magn Reson Med 74:772–784
20. Leu K, Boxerman JB, Cloughesy TF et al (2016) Improved leakage correction for single-echo dynamic susceptibility contrast (DSC) perfusion MRI estimates of relative cerebral blood volume (rCBV) in high-grade gliomas by accounting for bidirectional contrast agent exchange. AJNR Am J Neuroradiol 37:1440–1446
21. Boxerman JL, Prah DE, Paulson ES, Machan JT, Bedekar D, Schmainda KM (2012) The role of preload and leakage correction in gadolinium-based cerebral blood volume estimation determined by comparison with MION as a criterion standard. AJNR Am J Neuroradiol 33:1081–1087
22. Stokes AM, Skinner JT, Yankeelov T, Quarles CC (2016) Assessment of a simplified spin and gradient echo (sSAGE) approach for human brain tumor perfusion imaging. Magn Reson Imaging 34:1248–1255
23. Sourbron S, Heilmann M, Biffar A et al (2019) Bolus tracking MRI with a simultaneous T1- and T2*-measurement. Magn Reson Med 62(3):672–681
24. Lee MD, Baird GL, Bell LC et al (2019) Utility of percentage signal recovery and baseline signal in DSC-MRI optimized for relative CBV measurement for differentiating glioblastoma, lymphoma, metastasis, and meningioma. AJNR 40:1445–1450
25. Bell LC, Hu LS, Stokes AM, McGee S, Baxter LC, Quarles CC (2017) Characterizing the influence of preload dosing on percent signal recovery (PSR) and cerebral blood volume (CBV) measurements in a patient population with high-grade glioma using dynamic susceptibility contrast MRI. Tomography 3:89–95
26. Boxerman JL, Paulson ES, Prah MA, Schmainda KM (2013) The effect of pulse sequence parameters and contrast agent dose on percentage signal recovery in DSC-MRI: implications for clinical applications. AJNR Am J Neuroradiol 34:1364–1369
27. Hu LS, Eschbacher JM, Heiserman JE, Dueck AC, Shapiro WR, Liu S, Karis JP, Smith KA, Coons SW, Nakaji P, Spetzler RF, Feuerstein BG, Debbins J, Baxter LC (2012) Reevaluating the imaging definition of tumor progression: perfusion MRI quantifies recurrent glioblastoma tumor fraction, pseudoprogression, and radiation necrosis to predict survival. Neuro Oncol 14:919–930
28. Barajas RF, Chang JS, Sneed PK, Segal MR, McDermott MW, Cha S (2009) Distinguishing recurrent intra-axial metastatic tumor from radiation necrosis following gammaknife radiosurgery using dynamic susceptibility-weighted contrast-enhanced perfusion MR imaging. AJNR Am J Neuroradiol 30:367–372
29. Liao W, Liu Y, Wang X et al (2008) Differentiation of primary central nervous system lymphoma and high-grade glioma with dynamic susceptibility contrast-enhanced perfusion magnetic resonance imaging. Acta Radiol 50:217–225
30. Askaner K, Rydelius A, Engelholm S et al (2018) Differentiation between glioblastomas and brain metastases and regarding their primary site of malignancy using dynamic susceptibility contrast MRI at 3T. J Neuroradiol 46:367–372
31. Toh CH, Wei KC, Chang CN, Ng SH, Wong HF (2013) Differentiation of primary central nervous system lymphomas and glioblastomas: comparison of diagnostic performance of dynamic susceptibility contrastenhanced perfusion MR imaging without and with contrast-leakage correction. Am J Neuroradiol 34:1145–1149
32. Xing Z, You RX, Li J, Liu Y, Cao DR (2014) Differentiation of primary central nervous system lymphomas from high-grade gliomas by rCBV and percentage of signal intensity recovery derived from dynamic susceptibility-weighted contrast-enhanced perfusion MR imaging. Clin Neuroradiol 24:329–336
33. Valles FE, Perez-Valles CL, Regalado S, Barajas RF, Rubenstein JL, Cha S (2013) Combined diffusion and perfusion MR imaging as biomarkers of prognosis in immunocompetent patients with primary central nervous system lymphoma. AJNR Am J Neuroradiol 34: 35–40
34. Hartmann M, Heiland S, Harting I, Tronnier VM, Sommer C, Ludwig R, Sartor K (2003) Distinguishing of primary cerebral lymphoma from high-grade glioma with perfusion-weighted magnetic resonance imaging. Neurosci Lett 338:119–122
35. Nagy JA, Chang SH, Dvorak AM, Dvorak HF (2009) Why are tumour blood vessels abnormal and why is it important to know? Br J Cancer 100(6):865–869
36. Blasel S, Jurcoane A, Franz K, Morawe G, Pellikan S, Hattingen E (2010) Elevated peritumoural rCBV values as a mean to differentiate metastases from high-grade gliomas. Acta Neurochir 152:1893–1899
37. Halshtok Neiman O, Sadetzki S, Chetrit A, Raskin S, Yaniv G, Hoffmann C (2013) Perfusion-weighted imaging of peritumoral edema can aid in the differentialdiagnosis of glioblastoma mulltiforme versus brain metastasis. Isr Med Assoc J 15(2):103–105
38. Pekmezci M, Perry A (2013) Neuropathology of brain metastases. Surg Neurol Int 4(Suppl 4):S245–S255
39. Semmineh NB, Bell LC, Stokes AM, Hu LS, Boxerman JL, Quarles CC (2018) Optimization of acquisition and analysis methods for clinical dynamic susceptibility contrast MRI using a population-based digital reference object. AJNR Am J Neuroradiol 39:1981–1988
40. Paulson ES, Prah DE, Schmainda KM (2007) Correction of confounding leakage and residual susceptibility effects in dynamic susceptibility contrast MR imaging using dual-echo SPIRAL. In: Proceedings of the 45th Annual Meeting of the American Society of Neuroradiology and Neuroradiology Education and Research Foundation Symposium, Chicago, Illinois; June 7–14
41. Schmiedeskamp H, Straka M, Newbould RD, Zaharchuk G, Andre JB, Olivot JM, Moseley ME, Albers GW, Bammer R (2012) Combined spin- and gradient-echo perfusion-weighted imaging. Magn Reson Med 68(1):30–40